Characterization of atmospheric aerosols in the Antarctic region using Raman Spectroscopy and Scanning Electron Microscopy

César Marina-Montes[1], Luis V. Pérez-Arribas[2], Jesús Anzano1, Silvia Fdez-Ortiz de Vallejuelo[3], Julene Aramendia[3], Leticia Gómez-Nubla[3], Alberto de Diego[3], Juan Manuel Madariaga[3], Jorge O. Cáceres[*1]

[1] Laser Lab, Chemistry & Environment Group, Department of Analytical Chemistry, Faculty of Sciences, University of Zaragoza. Pedro Cerbuna 12, 50009 Zaragoza, Spain

[2] Laser Chemistry Research Group, Department of Analytical Chemistry, Faculty of Chemistry, Complutense University of Madrid. Plaza de Ciencias 1, 28040 Madrid, Spain

[3] Department of Analytical Chemistry, Faculty of Science and Technology, University of the Basque Country UPV/EHU. Leioa, Spain

ABSTRACT: The non-destructive spectroscopic characterization of airborne particulate matter (PM) was performed to gain better knowledge of the internal structures of atmospheric aerosols at the particle level in the Antarctic region, as well as their potential sources. PM and soil samples were collected during the 2016-2017 austral summer season at the Spanish Antarctic Research Station "Gabriel de Castilla" (Deception Island, South Shetland Islands). PM was deposited in a low-volume sampler air filter. Raman spectroscopy (RS) and Scanning Electron Microscopy with Energy-Dispersive X-ray Spectroscopy (SEM-EDS) were used to determine the elemental and molecular composition of the individual aerosol and soil particles. In most of the Raman spectra, two broad and overlapping bands appeared at ~1580 cm^{-1} (G or graphite peak) and ~1360 cm^{-1} (D or defect peak), identified as carbon due to combustion generated by large molecular organic carbon species and carbon soot. Filter spectra measured by these techniques revealed single and cluster particles made of different kinds of black carbon (BC), organic compounds such as polyestyrene, as well as minerals, with an anthropogenic (polyhalite, arcanite, niter, ammonium nitrate, syngenite and nitrogen, phosphorus, and potassium (NPK) fertilizer) and natural (sea salts, silicates, iron oxides, etc.) origin, respectively. In addition to the filter samples, forsterite and plagioclase were discovered in the soil samples together with magnetite.

Keywords: Antarctic region; Deception Island; Atmospheric aerosols; Black Carbon; Raman spectroscopy; Scanning electron microscopy; Energy-dispersive X-ray spectrometry

*Corresponding author. Jorge O. Cáceres. E-mail: jcaceres@ucm.es (J.O. Cáceres).

INTRODUCTION.

Aerosol particulate matter (PM) is a fundamental component in the atmosphere. These particles play a crucial role in the environment and health.[1-3] Firstly, aerosol particles are considered as climate drivers since they are involved in the radiative balance of the Earth, affecting the Earth´s energy budget.[4] Secondly, a strong correlation exists between hazardous heavy metals present in PM, i.e. Pb, Cd, Zn, etc., and human health-related impacts.[5,6]Atmospheric aerosols are able to travel thousands of kilometres in a limited period of time and have a typical duration of one year in the stratosphere, and one day to two weeks in the troposphere.[7] Thus, the Antarctic region, which acts as a global thermostat being one of the major pristine and isolated environments on Earth, is negatively affected by anthropogenic PM pollution from distant as well as local sources.[8] The composition of atmospheric PM can differ widely, depending on their natural (sea, earth erosion, biogenic emissions, volcanoes, etc.) and/or anthropogenic (fossil fuel combustion, mining, agriculture, etc.) sources.[9] Among anthropogenic sources, cruise tourism in the study area is particularly important.[10] For instance, Whalers Bay, located in the caldera of Deception Island, was the second most-visited place in the Antarctic Peninsula with more than 20,000 visitors during the 2016-2017 austral summer season.[11] Although aerosols have been abundantly studied in Antarctica,[12-15] their variable composition is still widely unknown.[7] Thus, it is essential to investigate their chemical composition, as well as their potential sources and impacts on the Antarctic environment.[16,17]

Both environmental and health effects of PM are linked to their elemental composition and their size distribution. However, these properties are not sufficient to estimate accurately their environmental consequences, since single particles are internally made up of various species. Consequently, PM chemical characterization of individual particles is needed.[18-20] Chemical characterization of individual particles through Raman spectroscopy is a powerful technique for improving the characterization of aerosols.

Raman spectroscopy (RS) is a simple rapid method which does not require sample treatment. It has been extensively used to characterize the chemical composition of airborne particulate matter.[20-23] Furthermore, Raman spectra can be used to identify the sources of such PM, since distinct kinds of carbonaceous particles are produced in the combustion of different fossil fuels, such as diesel, gasoline, coal or biomass burning. [24,25]

In this study, RS was used to determine particle specific composition as an indicator of potential sources of Antarctic aerosol samples. As a complementary technique, and in the interest of confirming the internal structure and chemical composition of PM, analysis by scanning electron microscopy (SEM) and Energy Dispersive X-Ray Spectroscopy (EDS) were also implemented. Since RS is intended to characterize covalent compounds (carbonates, sulphates, nitrates, oxides, etc.), SEM-EDS is an appropriate complement to identify the remaining ionic particles, such as NaCl, as well as to confirm Raman analyses. The combination of these three robust techniques (RS & SEM-EDS) is perfectly adapted for identifying the chemical and structural composition of aerosol samples.[26-28]

This paper focuses on the investigation by RS and SEM-EDS of the chemical composition of individual aerosol and soil particles collected during the austral summer season in the Antarctic region. This information is of great significance for studying the environmental impact of anthropogenic aerosols on the icy continent, as well as for anticipating their influence on climate change.

EXPERIMENTAL SECTION

Materials and Methods.

Site description and sampling.

Samples of atmospheric aerosols were collected from December 2016 to February 2017 on Deception Island, specifically in the surroundings of the Spanish Research Base "Gabriel de Castilla" (62°58′09″S, 60°42′33″W). This island has one of Antarctica´s safest harbours and is the caldera of an active volcano. It is part of the volcanic South Shetland Islands archipelago, located north of Antarctic Peninsula (Figure 1). Although multiple PM samples were collected at the sampling point, only 15 samples were used in this study. Each PM_{10} sample was collected during 24 hours in circular quartz microfiber filters of 47 mm diameter (Munktell) using a low volume sampler (Derenda LVS 3.1; 2.3 m^3/h). After the 24 h period, the samples were meticulously stored with laboratory film in petri dishes using nitrile globes and sterilised tweezers. The European Norm was used to determine the mass concentration by gravimetry. [29] Additionally, random top soil samples were collected close to the PM sampling point. These soil samples were taken in

order to characterize their geochemical fingerprint to obtain spectroscopic references (mineral composition) and thus identify sources for the particles detected in the aerosols.

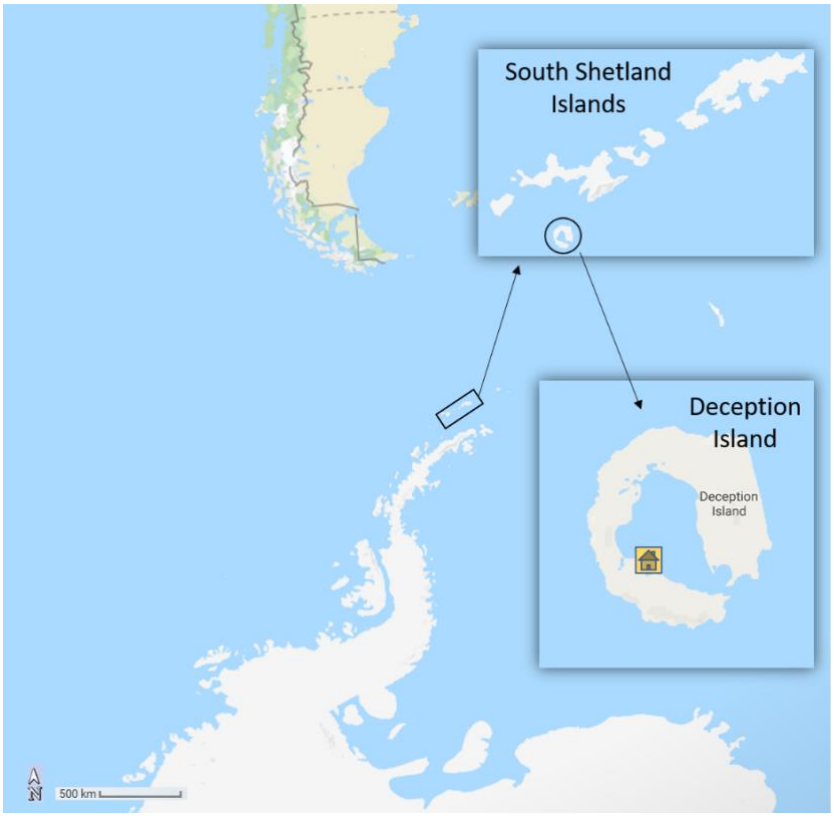

Figure 1. Map of Deception Island with the exact location of the Gabriel de Castilla Spanish Antarctic Research Station. The yellow house shows the position of the station.

Experimental setup.

RS measurements were carried out by means of a Raman InVia spectrometer (Renishaw) provided by StreamLine image tools. Spectra acquisition was done using Leica 50× N Plan (0.75 aperture) and 20× N Plan EPI (0.40 aperture) magnification long-range objectives. The microscope with a camera coupled used a Prior scientific motorized stage (XYZ) controlled by a joystick that facilitates focusing on and searching for points of interest. Besides, the device is equipped with a class 1 enclosure for avoiding artificial or sunlight effects. In addition, the instrument is installed on an antivibratory table.

In this study, RS analysis was carried out using three excitation lasers, 532 nm, 633 nm and 785 nm. The laser power was adjusted by means of density filters to below 150 µW to avoid thermo-decompositions of the sample. Analyses were always performed using from 0.0001 % to 10% of the power laser. Raman spectra of the cleaned filters (circular quartz microfiber filters, Munktell) were taken using all the excitation lasers in order to obtain blanks of the analytical procedure.

The calibration of the equipment was performed twice per day with a silicon slice, using its characteristic bands (520.5 cm^{-1}). The quality of measurements was assessed by an internal calibration using the same silicon chip. Moreover, the laser beam was centred twice per day to assure an appropriate analysis. The mean spectral resolution was around 1 cm^{-1}, and the spectra were obtained in a range of 100–1800 cm^{-1} or up to 3000 cm^{-1}. All the point-by-point measurements were collected using the following acquisition parameters: point analysis with a laser power of less than 10% exposure time between 2 and 10 s and between 1 and 30 accumulations. In order to improve the quality of the spectra, the measurements were set up modifying these parameters within this range.

Omnic 7.2 (Thermo Fisher-Nicolet, Madison, USA) and Wire 4.2 (Renishaw, UK) software were used for data analysis. Interpretation of the results was done by comparison of the collected Raman spectra with those of pure standard compounds from our own databases,[30] the bibliography and from the RRUFF database.[31]

The Raman images were collected on spots of approximately 500x500 microns. This allows performing fast 2D Raman images of the filter samples. In order to take the Raman images, the region of interest has to be defined and then an X step is performed. In this case, steps between 10-20 microns were used, always employing a 20x objective for the images. The methodology applied was to define as many seconds and accumulations as possible to ensure the best signal- to- noise ratio to obtain each Raman map time less than 12 hours. Therefore, the acquisition conditions varied from map to map depending on the region size and the material Raman response. The most commonly applied conditions were 5-15 seconds and 1-5 accumulations. Once the Raman image was acquired, some automatic treatments were applied to the dataset using a systematic procedure in order to guarantee the repeatability of the experimental results. First of all, the baseline automatic correction was performed to smooth the fluorescence background in the whole spectra set. Then, cosmic ray removal was carried out using the Nearest Neighbour option which works comparing the spectrum with the nearest ones and determining correlation coefficients for each spectrum with all its spatial neighbours in order to select the most similar neighbour spectrum. In this way, as the cosmic rays are random through the comparison they would be not taken into account.

SEM filter analyses were carried out using a microscope (model HitachiS-3000N). EDS analyses were performed with an attached EDS analyser (Oxford Instruments INCAx-sight). This SEM instrument offers the possibility to image morphological surface features of PM at high spatial resolution, down to 1 μm, with a

large depth-of-field, resulting in accurate 3D images of the sample features. The accelerating voltage was preset at 20 kV. The connected EDS provided elemental composition of the sample, which was limited to Z > 10.

Since this multianalytical methodology requires a reduced number of collected particles, it provides useful information about the elemental composition, size and shape of PM. Therefore, the combined technique is effective when differentiating particles originating from different sources.

Statistical analysis.

PLS-Toolbox v.7.0.2 (Eigenvector Research, USA) implemented in MATLAB 2010 software (The Mathworks, MA, USA) was used on selected Raman spectra for performing the statistical analyses such as principal component analysis (PCA).

RESULTS AND DISCUSSION

The composition of the clean filters is sensitive to RS. For that reason, the Raman spectra of the filters was first measured in order to have a blank for reference. This spectrum is shown in Figure 2b, where broad bands around 480, 610, 800, 980 and 1890 cm^{-1} are clearly observed due to the silicic nature of the fibers composing the filter.

The view of the various particles through the microscope of the Raman spectrometer evidenced diverse sizes, from a couple of microns to more than 30 microns. This observation is important because in some cases the particle size was lower than the diameter of the laser spot (typically 2.5-0.8 microns when using a 50x or 20x objective, depending on the laser wavelength) used to obtain the Raman spectra. For such cases, the spectrum of the particle was obtained together with part of the background spectrum of the filter itself. This situation is shown in Figure 2c, where the two main bands of polystyrene (at 1001 and 1602 cm^{-1}) are clearly seen together with the Raman background coming from the signals provided by the filter. In all cases, the particles of this plastic were lower in size (less than 5 microns) than the spot size of the laser and similar spectra to that shown in Figure 2c were obtained, indicating a significant presence of microplastic particles in the filtered aerosols.

Other particles were larger than the diameter of the laser spot and the focusing with the microscope could be centred on the particle without obtaining the Raman background signals from the filters. This is the case shown in Figure 2a, where only the Raman spectrum of carbon is shown with its D and G bands. The presence of carbon

particles was observed in all of the filters and in significant amounts relative to other white particles. Moreover, the Raman response of these carbon particles was different, indicating that several carbon particles (particles from different sources) were trapped by the filters. This experimental evidence led us to study in-depth the nature of such particles.

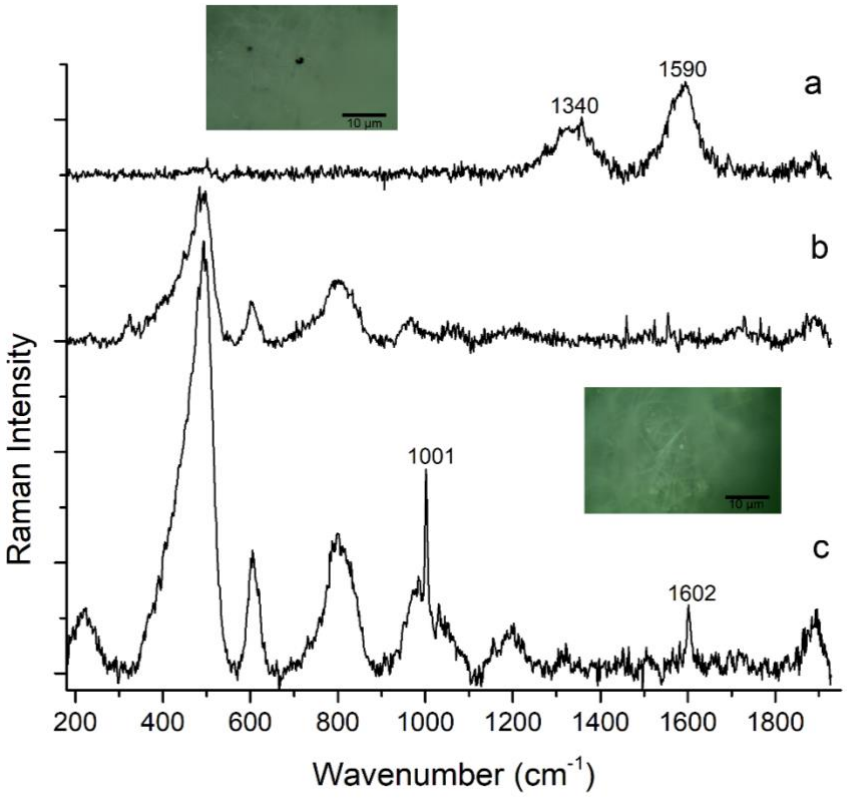

Figure 2. Raman spectra performed on the filters a) carbon particle signal, b) filter signal and c) filter signal with a polystyrene particle signal.

Raman spectra of Black Carbon in aerosol samples.

The black carbon (BC) consists of elemental carbon and some hydrogen and oxygen. It includes different components such as soot particles, graphitic carbon and/or organic carbon coming from partially combusted biomass. Nowadays, it is considered the second most important pollutant affecting climate change.

Different aerosol BC particles were analysed and the 1050-1850 cm^{-1} range of wavenumbers of their Raman spectra were mathematically treated, using a Raman two-band fitting procedure, to determinate the different types of BC present on the filters. Figure 3 shows four of these different Raman profiles obtained from several analysed particles. As previously described in other publications,[24,25,32] there are two broad

overlapping bands at ~1585 cm^{-1} and ~1360 cm^{-1}. The first band corresponds to the so-called G band, while the second band corresponds to the so-called D band or defect peak. Both bands have different forms and maximum values in their wavenumbers depending on the nature of carbon.

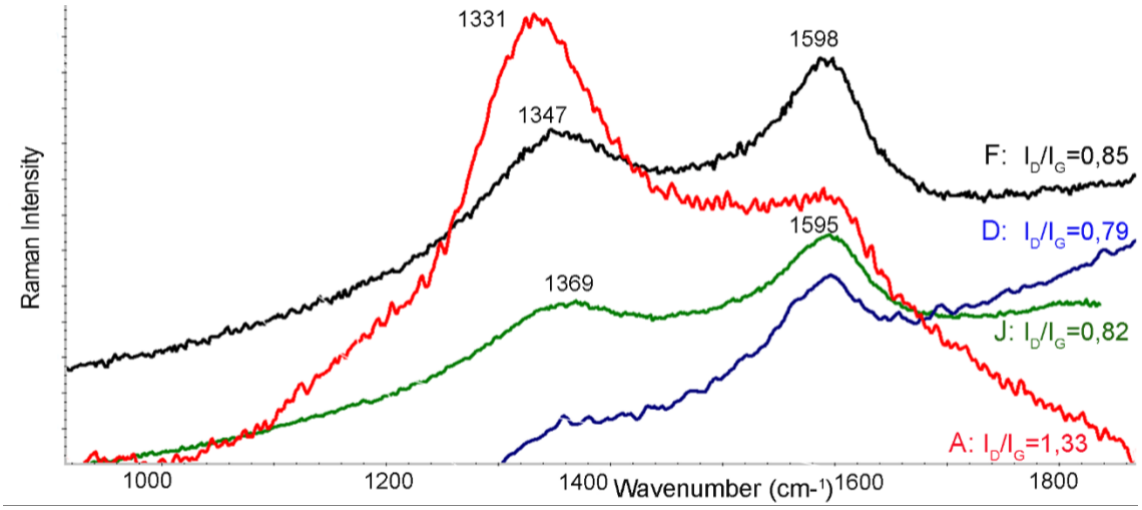

Figure 3. Two-peak fitting results from Raman spectra of four BC particles (code spectra: A, D, F and J) from different Antarctic aerosol samples.

The Raman spectra in the above-mentioned range of four selected BC particles (named A, D, F and J in Figure 3) taken from the filter samples are those that exhibit greatly varying relative intensities and widths. The ratio of the D to J peaks gives the relative amount of edge to volume of the crystals.[24] The J peak is the E_{2g} mode of bulk crystalline graphite. In contrast, the D peak appears when the graphite breaks down near the crystal edges. Both peaks indicate that BC particles are formed by amorphous carbon, which is a combination of crystalline graphite and a non-graphite element. The shapes and intensities of both bands are also functions of the morphology and sample composition. The spectra of F, D and J present a similar shape, and the high signal intensities between the two main peaks of the observed spectra have been assigned to the G band. This band is associated with the ordered graphitic carbon content of various compounds, such as soot, and organic molecules such as humic acids, graphite, etc.

I_D/I_G was estimated as an indicator of the degree of BC disorder.[25,33] The intensity ratios of the D band to the G band for the A spectrum (main Raman band at 1331 cm^{-1}) was higher (1.33) than the D, F and J spectra (0.79-0.85 and main Raman band at 1598 cm^{-1}). A previous study found similar values for the spectra parameter I_D/I_G, as in our D, F and J spectra, for the Raman features of carbon particles coming from biomass

burning and diesel emissions.[25] In contrast, other researchers found higher I_D/I_G values for soot samples (higher or similar to those determined for sample A in this work).[33,34]

These I_D/I_G values enabled us to create Raman images from selected areas in the filters with significant abundances of BC particles. As an example, Figure 4 shows such a Raman spectroscopy image, where the different colors (plotted as a function of the I_D/I_G values, red being the highest I_D/I_G ratios and blue the lowest) clearly show the rounded shape of the particles and how there is no zonification among them. In contrast, the different BC particles seem to be randomly trapped in the filters. However, it is still difficult to identify the different sources of the BC in this case.

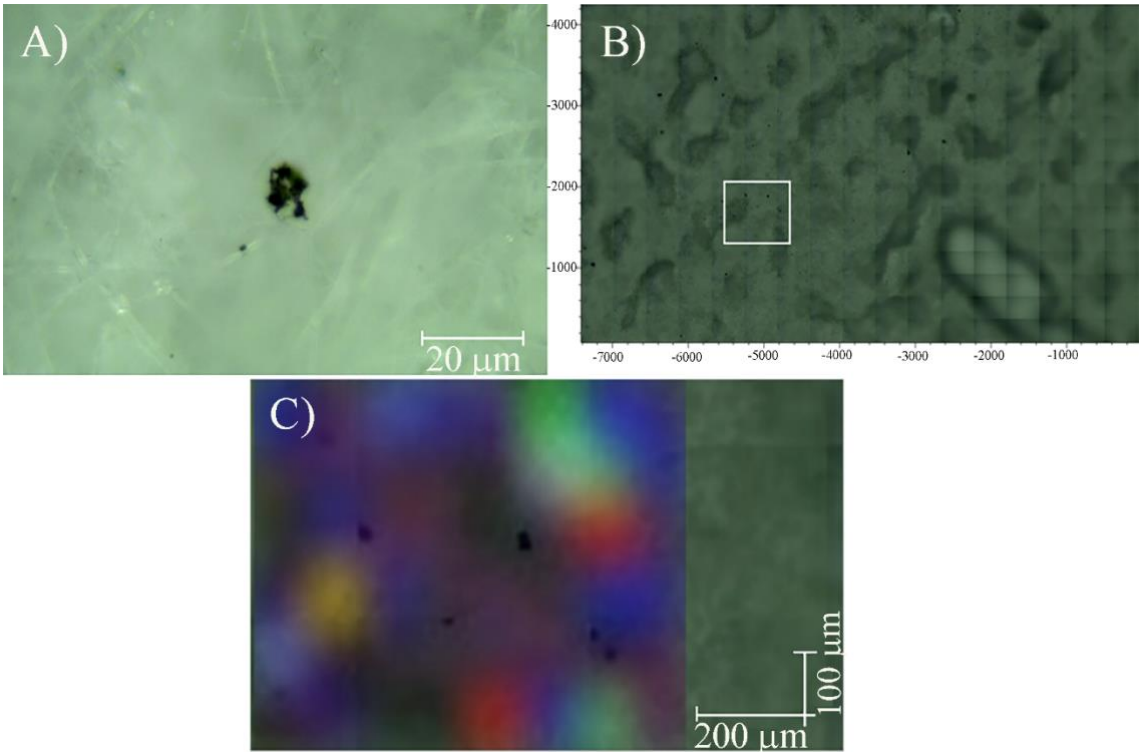

Figure 4. Raman imaging analysis (laser at 532 nm) of a filter showing the distribution of four BC particles in an area of 800x500 microns.

Taking into account the D and G bands of the A, D, F and J spectra (see Figure 3), it is clear that there are different disorder levels in the analyzed BC. This indicates the existence of different kinds and sources of BC particles in the Antarctic PM sample.

In order to obtain more information about these different types of BC present in the filter samples, a chemometric analysis of the data was performed by Principal Component Analysis (PCA). PCA, as a non-supervised technique, is the most commonly used technique to reduce the dimension of large datasets. Mathematically, PCA uses a covariance matrix, constructed according to the dispersion of the measured variables, to

calculate the so-called “eigenvalues” and “eigenvectors”. Mutually orthogonal Principal Components (PCs) are calculated by the linear combination of the original variables.

Ten spectra with only the characteristic carbon Raman bands and without the Raman background of the filter or fluorescence were selected. The selected Raman spectra were not pre-processed. The PCA was carried out using the spectral region corresponding to 1197–1663 cm^{-1}.

As the results did not significantly change when a fourth PC (only an extra 2.5% of explained variance) was considered, the model with the three first PCs (49%, 29%, and 16% of explained variance, respectively) was finally selected to describe the whole set of the Raman spectral variability in the carbon region. The scatter plot obtained is shown in Figure 5. This shows the representation of the scores in the space formed by two of the most important PCs.

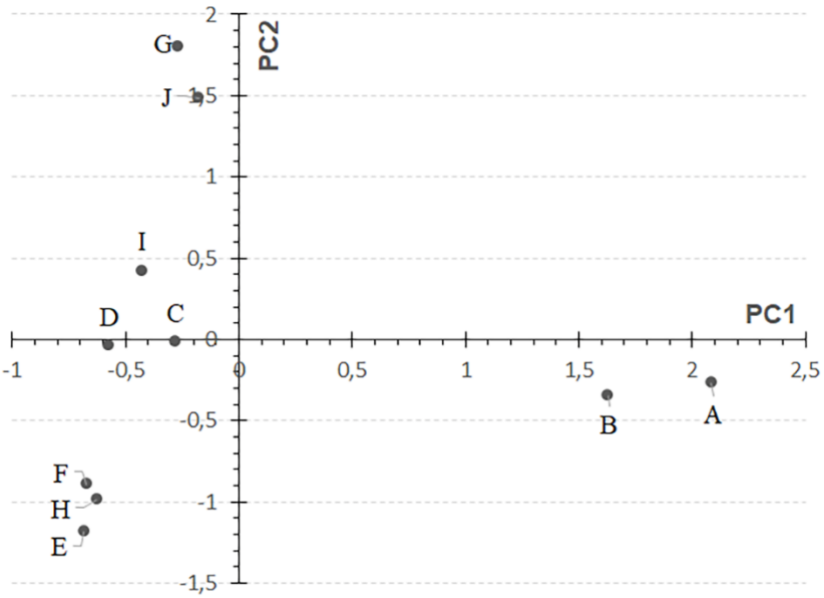

Figure 5. Scores from statistical analysis from Raman spectra (Code spectra: A, B, C, D, E, F, G, H, I and J) of BC particles from PCA of two PCs.

In this PCA plot, the distribution of the scores reveals the existence of at least four different behaviours of Raman spectra, which implies four different BC particles. The first one includes the A and B spectra (PC1positive value and PC2 nearly neutral), a second one for E, F and H (negative PC1 and PC2 values), a third one for C, D and I (negative PC1 and nearly neutral PC2) and a fourth one for G and J (negative PC1 and

positive PC2 values). PC1 seems to be related to the Raman intensity of the D band of BC, and PC2 to the shape and intensity of the G peaks.

Since it has been observed during consecutive Antarctic field campaigns that the study area is well-known as an attractive Antarctic cruise destination (chinstrap penguin colonies, geothermal bathing, etc.), one of the potential sources of these three different BC particles (those with negative PC1 values) is tourist cruise emissions. Some of these daily tours even stay overnight at the island with the diesel engines working to produce the electricity they need. The remaining BC source probably corresponds to organic waste incineration that produces a significant amount of soot particles, characterised by Raman spectra like that named A.

Raman spectra of non-Black Carbon aerosol samples.

The search for non-BC particles in the filters revealed a great variety of sizes and shapes, alone or close to BC particles. As an example, Figure 6 shows a Raman spectrum where three minerals, hematite (Fe_2O_3), magnetite (Fe_3O_4) and carbon, are simultaneously present in a particle of a diameter greater than 30 microns that inhibits the appearance of the Raman background of the filter materials. The major source of Fe oxide particles in the study site is volcanic soil. Fe oxides can correspond to primary magnetites from the magmatic rocks of Deception island (magnetite) or secondary goethite in the soils created during the aerobic weathering of these rocks (hematite).

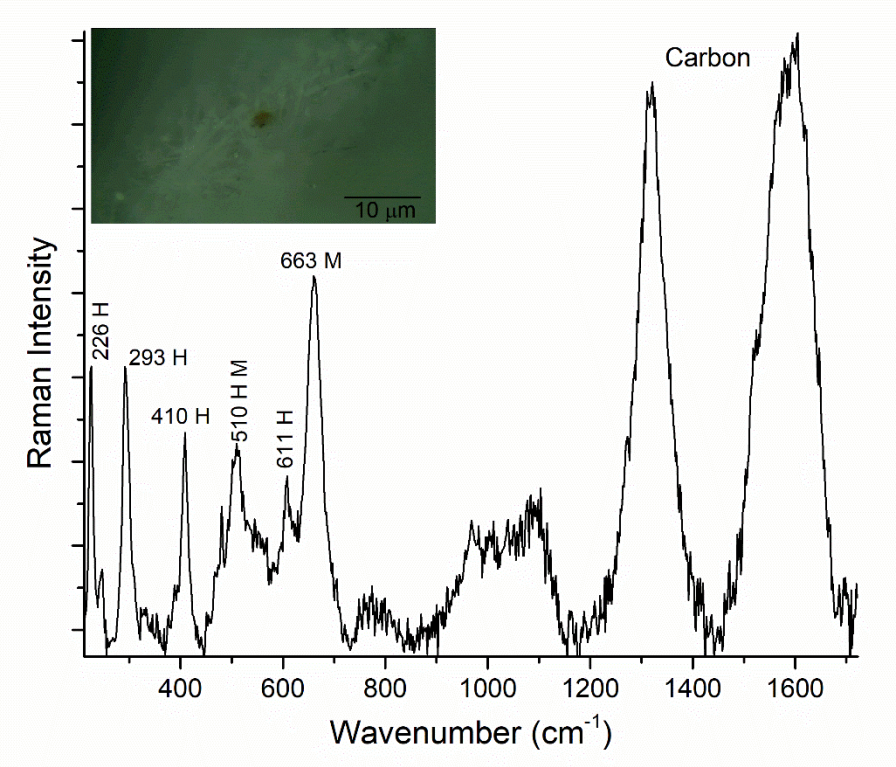

Figure 6. Raman spectra of hematite (H), magnetite (M) and carbon from an Antarctic aerosol sample.

Another white particle with a non-rounded form, mostly a cluster of several grains, showed a very complex Raman spectrum, as shown in Figure 7. To decipher the minerals, present in the spectrum, the main signals around 1000 cm^{-1} were decomposed in individual bands. This mathematical treatment led to the conclusion that syngenite ($K_2Ca(SO_4)_2 \cdot H_2O$, Raman bands at 601, 633, 661, 982 and 1004cm^{-1}) was present,[35] together with gypsum ($CaSO_4 \cdot 2H_2O$, main Raman band at 1008 cm^{-1}) probably mixed with basanite ($CaSO_4 \cdot ½H_2O$, main Raman band at 1017 cm^{-1}).[36] Moreover, the band at 1050 cm^{-1} shows a FWHM=25 cm^{-1}, that belongs to nitrocalcite ($Ca(NO_3)_2 \cdot 4H_2O$).[37] The origin of these minerals can be attributed to the hydrothermal and volcanic activity of the island.

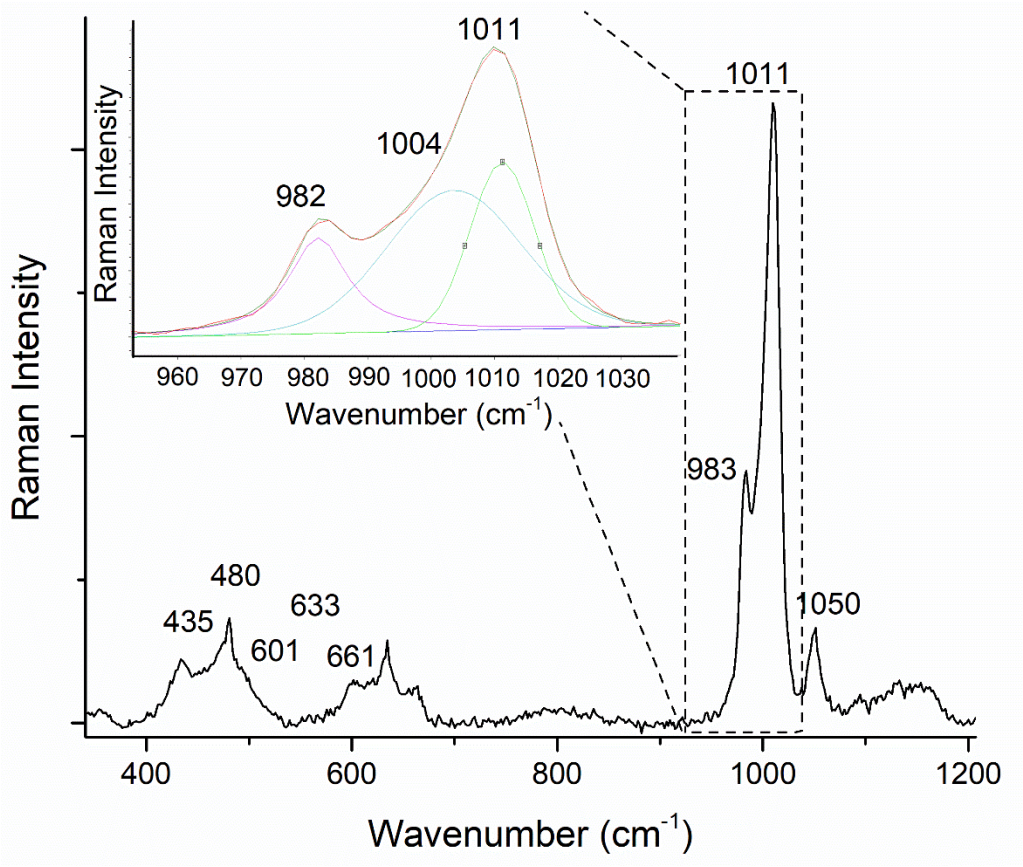

Figure 7. Raman spectrum of a clustered particle with syngenite, gypsum+basanite and nitrocalcite.

Another complex Raman spectrum obtained on a white particle is shown in Figure 8. It contains a mixture of Fe-polyhalite ($K_2FeCa_2(SO_4)_4 \cdot 2H_2O$; Raman bands at 437, 474, 635, 659, 982 and 1010cm^{-1}), the potassium sulphate arcanite (K_2SO_4; Raman bands at 454, 612, 983cm^{-1}) and niter (KNO_3) with a Raman band at 1049 cm^{-1} with a FWHM=10 cm^{-1}.[38] The bands at 233, 318, 349, 558 and 788 are close to secondary bands of complex phosphate compounds, its main Raman band overlapped by the feature at 982 cm^{-1}.The sulphate bands were the most intense, followed by the nitrate band.

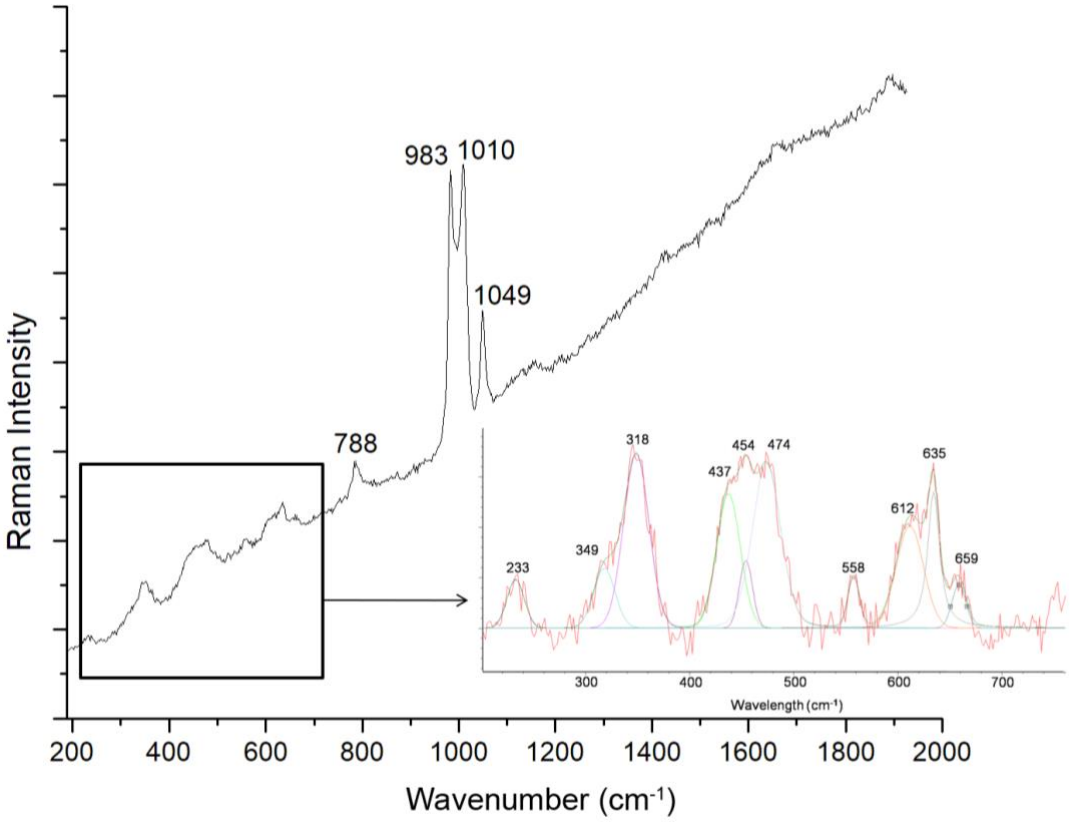

Figure 8. Raman spectrum of a white particle containing Iron-Polyhalite, arcanite and niter from an Antartic aerosol sample.

Another commonly detected Raman spectrum is shown in Figure 9. Again, to solve the complex features, the broad bands were mathematically treated to decompose them into individual bands. The main Raman signal is made up of three bands that correspond to magnesio-cocapite ($MgFe^{3+}_4(SO_4)_6(OH)_2.20H_2O$, main Raman bands at 1002 and 1025 cm^{-1}) and gypsum+bassanite due to the signal at 1011 cm^{-1}. The most important secondary broad band was also decomposed, observing several bands that indicate the presence of magnesio-copiapite and a mixture of gypsum and basanite.[36,39]

Apart from the above-mentioned compounds, the complicated mixture of bands suggests that the presence of methanesulfonate (MSA) also has to be considered. Na methanesulfonate shows Raman bands at 354, 560, 781, 986, 1052, among others.[40]

The repeated identification of the three bands at 983, 1004-1010 and 1050 always together in the particles led to the conclusion that they have the same origin. Fertilizers display these three bands, attributed to potassium nitrate, urea, and potassium sulphate. The relative intensity of the three bands is different for each fertilizer, depending on the manufacture process and of the labelled NPK composition (% of nitrogen, phosphorous, sulphur, and potassium).[41] However, several studies of Antarctic and Arctic particles

using Raman spectroscopy have shown similar spectra with bands at ~ 985, 1008-1010 and 1050 cm^{-1}.[22,42] Unfortunately, there is no agreement about the actual composition or the source of the detected compounds. Some references relate the presence of sulphates and nitrates to high phytoplankton activity, mainly in summer.[22,43] Others,[42] in contrast, point to the reaction between sea spray aerosol and acid gases (HNO_3 and HSO_4) as the trigger for the formation of these salts. Additionally, these compounds may have their natural origin in the volcanism of the island. Besides, the erosion of sulphate- rich soils should also be considered.[44]

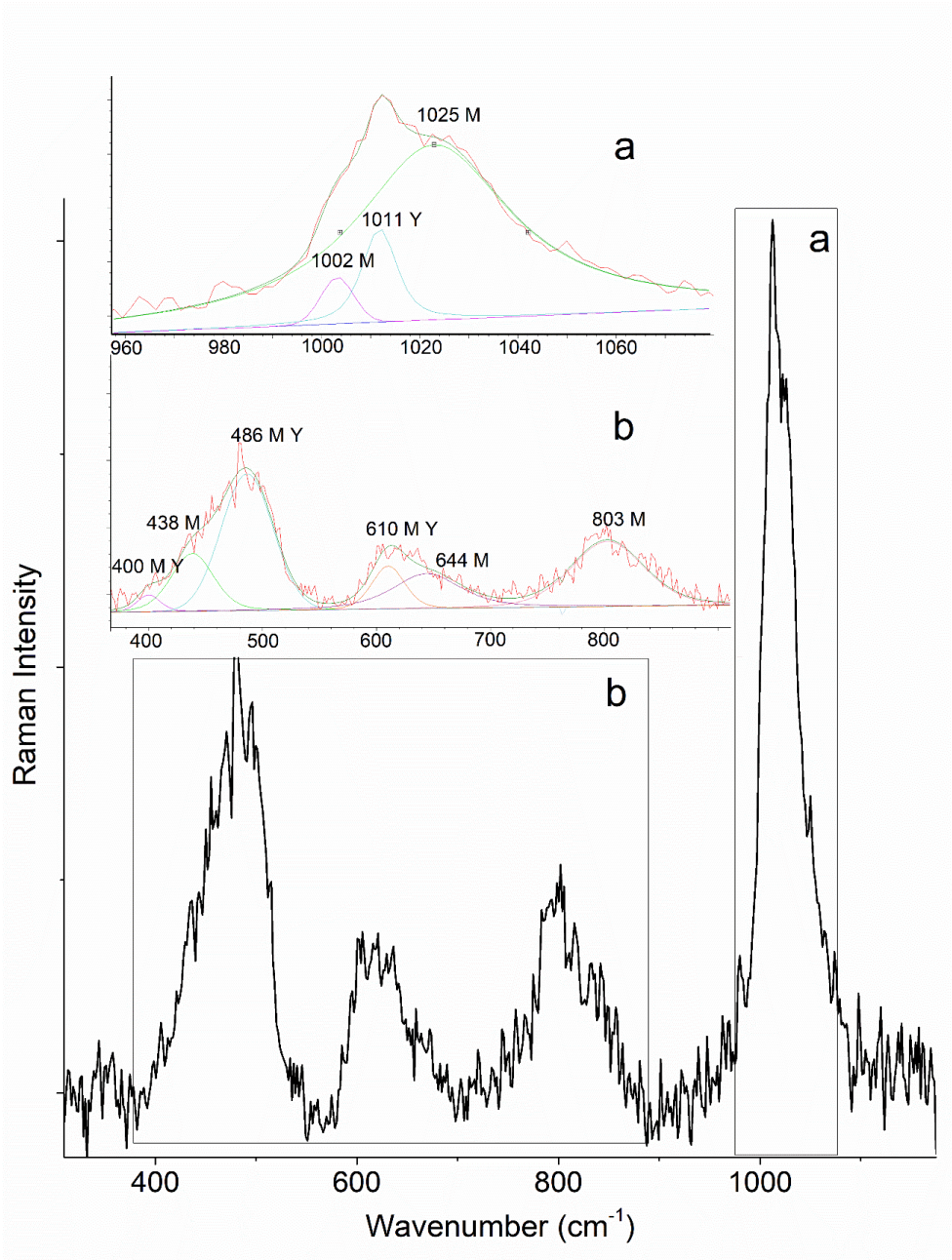

Figure 9. Raman spectrum of a white particle containing magnesio-copiapite (M), gypsum and basanite (Y) from a cluster of particles in an Antarctic aerosol sample. The main (b) and the secondary broad bands were decomposed in individual bands to help in the identification of the minerals simultaneously present in the complex particle.

Figure 10 shows a singular Raman spectrum with intense generic bands with contributions from proteins (amino acids) and lipids, such as 622 (Phenylalanine), 643 (Tyrosine), 759 (tryptophan), 830 (Tyrosine), 853 (Tyrosine), 1003 (Phenylalanine), 1127 (C-N, C-C stretching in proteins), 1200-1300 cm^{-1} (Amida III), 1447 (CH_2 deformation for lipids) and 1669 (Amide I) cm^{-1}. These were identified in the Raman spectra suggesting the presence of a possible bacteria, as described in the literature.[45]

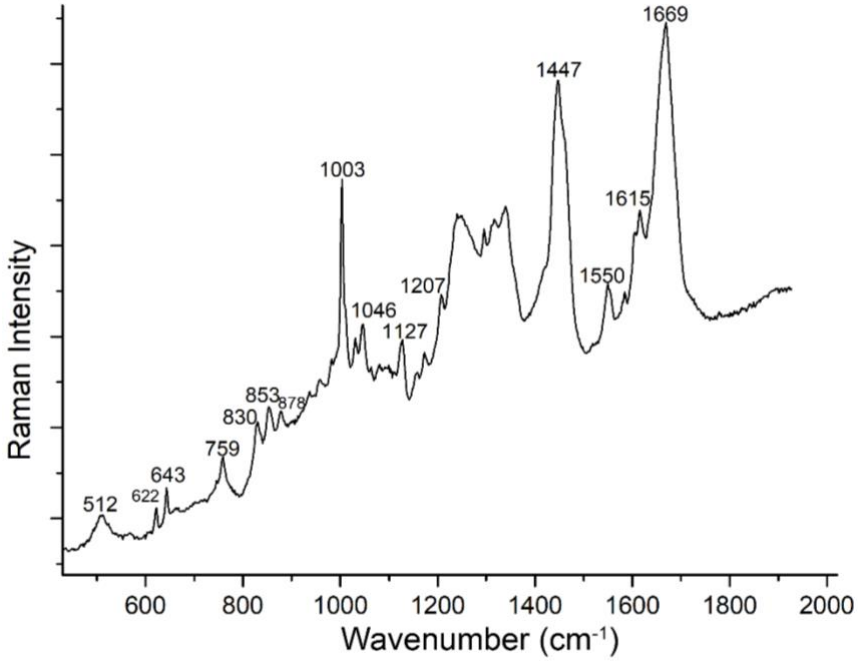

Figure 10. Raman spectrum of a possible biological(bacteria) particle from Antarctic filter sample.

Raman spectra of soil samples.

Raman analyses were also performed on the Antarctic soil samples, aiming to detect some of the minerals found in the particles trapped in the filters. By this means, mainly silicates were found. For instance, the olivine mineral forsterite (Mg_2SiO_4) was identified through its main Raman peaks at ~820 and ~854 cm^{-1} (Figure 11). Additionally, plagioclase ($(Na,Ca)(Si,Al)_4O_8$) was also detected due to its main Raman bands at 475, 510 and 999 cm^{-1}. Finally, the iron oxide magnetite (Fe_3O_4) was detected in the soil by means of its main Raman band at 669 cm^{-1}. From these mineral phases, only magnetite was detected in the filters, but the silicate minerals cannot be discarded because the siliceous nature of the filters can inhibit critical Raman signals of silicates that could eventually be trapped.

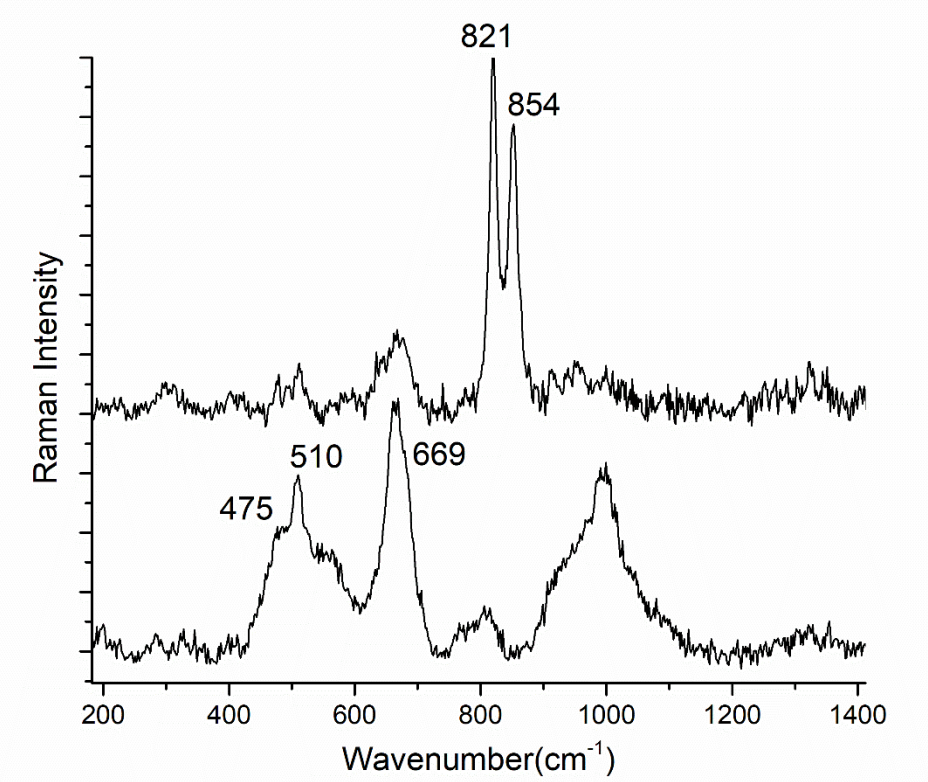

Figure 11. Raman spectra of an olivine mineral with the typical double bands at 821 and 854 cm^{-1}, and of a plagioclase together with magnetite (band at 669 cm^{-1}).

SEM-EDS analyses of filter samples.

The results obtained by SEM-EDS analyses show the presence of particles with different elemental compositions. A general morphological overview of the shapes of the particles found in the filters is presented in Figure 12A. Furthermore, different particles with variable compositions were detected (see Figure 12B, C, D and E). The EDS analyses of these strains provided the elemental composition in percentage weight of each element for four of these particles (Table 1).

Table 1. Element weight (%) obtained by Energy – Dispersive Spectrum K_α analysis of PM samples.

Spectrum	C	O	Na	Mg	Si	Cl	Cu	Al Ca	Ti	Fe
B (BC)	38.92	37.02	2.55	0.41	17.46	2.83	0.81			
C (NaCl)		36.71	30.24		6.61	26.44				
D (SiO_2)		62.35	8.81		22.11	6.73				
E (Fe Oxide)	8.74	53.02	2.43	2.55	17.82	0.66	0.73	5.58 3.08	0.88	4.51

According to the % values presented in Table 1, a tentative mineral composition was proposed and compared with the Raman observations previously described. On the basis of the chemical composition and shape of PM obtained through these analyses, the particles were divided into two groups: anthropogenic and natural.

Anthropogenic.

BC particles have their origin in local emissions, particularly in the incomplete combustion of diesel and biomass burning. The shape of these particles depends on different aspects, such as the burning conditions and fuel type. Figure 12B illustrates the amorphous aspect of a BC particle. As observed by SEM, these soots are made up of multiple small spheres of carbon. The major contribution was from elements such as C, Si and O, whereas Na, Cl and Mg were also present in very small concentrations (Table 1B). The contribution of Si and O corresponds to the quartz fiber filters; therefore, the most significant element is C.

Natural.

In the study, natural sources of PM include sea salt and crustal dust. These particles were mostly composed of sodium chloride, quartz and iron oxides.

Sodium Chloride.

The elements detected, such as Na and Cl, are related to the presence of sea salts. Sodium chloride particles and their characteristic tablet-like shape are shown in Figure 12C. They account for most of the particles collected on the filters. These particles were not detected by RS because this technique is not sensitive to ionic bonds.

Quartz (Silicate minerals).

Si and O were detected in the clusters presented in Figure 12C. As shown in Table 1D, the proportion of Si and O does not correspond to the SiO_2 from the quartz fiber filters; this suggests the presence of silicates in the air of the island. These particles have their origin in the resuspension of the volcanic basalt soil on the island. As shown in Table 1D, they are basically Si and O, with traces of Na and Cl. As stated before, these particles are hard to detect clearly due to the interference of the filters, but their presence has been confirmed.

Fe Oxides.

These particles were rich in Fe and O with traces of elements such as Na, Mg, Si, Cl, Cu, and Ca (Table 1E). Additionally, important amounts of C, Al and Ti were found. Their irregular shape is shown in Figure 12E. As previously mentioned, the origin of the particles is the volcanic soil on Deception Island. RS has detected both iron oxides, hematite and magnetite, in agreement with the SEM-EDS results.

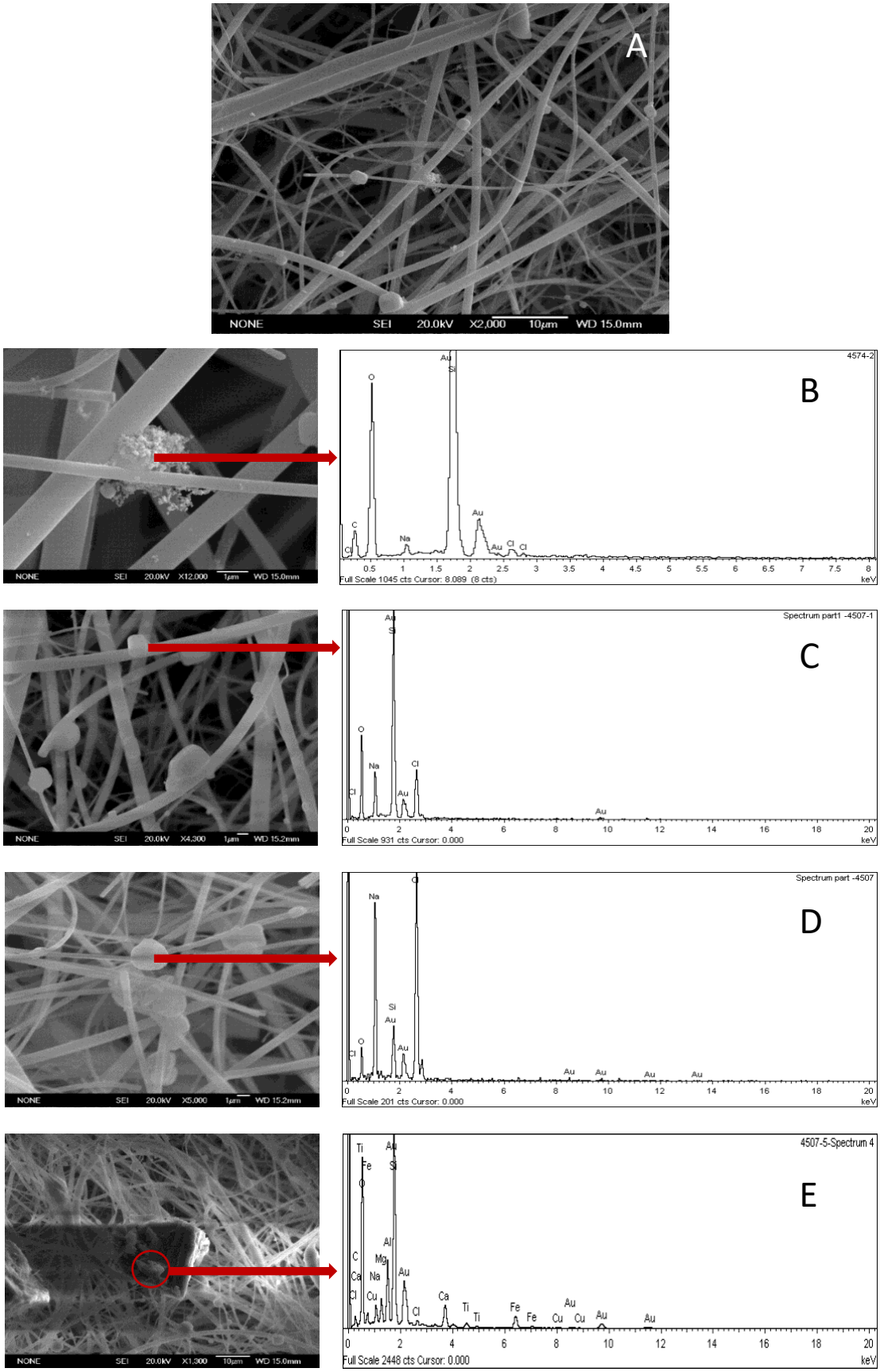

Figure 12. SEM-EDS spectra: (A) General morphological overview of PM particles in the quartz fiber filter; (B) Black Carbon particle and amorphous shape; (C) Sodium Chloride particle and tablet-like shape; (D) Quartz particle; (E) Iron oxide particle with traces of elements such as C, Na, Mg, Si, Cl, Cu, Al, Ca and Ti.

CONCLUSIONS

Antarctic particulate matter and soil measurements were conducted on samples collected during the austral summer 2016–2017 at the Gabriel de Castilla Spanish Research Station on Deception Island. The specific composition of the samples has been determined using Raman spectroscopy together with Scanning electron microscopy and Energy Dispersive X-ray spectrometry.

Raman analysis of aerosol samples revealed different kinds of black carbon particles present in the air of the island. This implies different potential sources of this pollutant in the area of study, the main ones being cruise tourism and waste incineration. Besides, Raman analysis of non-BC particles in the filters demonstrated the presence of bacteria as well as different anthropogenic compounds, such as microplastics (polystyrene) and minerals (polyalite, arcanite, niter, ammonium nitrate, syngenite and NPK fertilizer). To the best of our knowledge, these are the first aerosol measurements of microplastic (polystyrene) and fertilizer particles in the Antarctic atmosphere. In the case of soil particles, Raman spectra revealed that these were mainly composed of forsterite, plagioclase and magnetite. Additionally, Scanning Electron Microscopy and Energy Dispersive X-ray spectrometry confirmed the existence and the composition of amorphous carbon, as well as the presence of sea salts, silicates and iron oxides.

Air pollution, caused by the presence of BC, microplastic and fertilizer particles, can cause serious environmental problems for the Antarctic ecosystems as well as for the climate of this region. For instance, the presence of fertilizer particles together with the increasing trend of higher temperatures in the Antarctic Region will allow alien species to more successfully invade the Antarctic ecosystems. This disturbance, in addition to affecting the native Antarctic flora, will undoubtedly also affect the fauna.

It is important to point out that the long-term pollution and short-term climate effects on Antarctica cannot be inferred based on the results of this study. However, this investigation demonstrates that environmental pollution is a fact in the Antarctic region. Thus, successful characterization and regular monitoring of single particles is crucial for a better understanding of their potential environmental impacts on the Antarctic region.

AUTHOR INFORMATION

Corresponding Author

*J.O. Cáceres. Email:jcaceres@ucm.es.

Notes

The authors declare no competing financial interest.

ACKNOWLEDGMENTS

The authors gratefully acknowledge the following Spanish universities for facilities and material resources: University of Zaragoza, Complutense University of Madrid and University of the Basque Country. This project forms part of the Spanish Ministry of Science research program (CTM2017-82929-R & PID2020-112570RB-C21) in collaboration with the Government of Aragon proposal E23_17D and E49_20R. CMM's work was funded through a predoctoral contract (FPI) granted by the Spanish Government. Financial support from the European Social Fund & University of Zaragoza is acknowledged. The authors thank the military staff at the Gabriel de Castilla Spanish Antarctic research station for help with the installation of equipment and sample collection. Figure 1 has been taken from Google Earth Pro.

REFERENCES:

(1) Fuzzi, S.; Baltensperger, U.; Carslaw, K.; Decesari, S.; Denier van der Gon, H.; Facchini, M. C.; Fowler, D.; Koren, I.; Langford, B.; Lohmann, U.; Nemitz, E.; Pandis, S.; Riipinen, I.; Rudich, Y.; Schaap, M.; Slowik, J. G.; Spracklen, D. V.; Vignati, E.; Wild, M.; Williams, M., et al. *Atmos. Chem. Phys.* **2015**, *15*, 8217-8299.

(2) Bates, J. T.; Fang, T.; Verma, V.; Zeng, L.; Weber, R. J.; Tolbert, P. E.; Abrams, J. Y.; Sarnat, S. E.; Klein, M.; Mulholland, J. A.; Russell, A. G. *Environmental Science & Technology* **2019**, *53*, 4003-4019.

(3) Pöschl, U. *Angewandte Chemie International Edition* **2005**, *44*, 7520-7540.

(4) Nielsen, I. E.; Skov, H.; Massling, A.; Eriksson, A. C.; Dall'Osto, M.; Junninen, H.; Sarnela, N.; Lange, R.; Collier, S.; Zhang, Q.; Cappa, C. D.; Nøjgaard, J. K. *Atmos. Chem. Phys.* **2019**, *19*, 10239-10256.

(5) Csavina, J.; Field, J.; Taylor, M. P.; Gao, S.; Landázuri, A.; Betterton, E. A.; Sáez, A. E. *Science of The Total Environment* **2012**, *433*, 58-73.

(6) Nel, A. *Science* **2005**, *308*, 804.

(7) IPCC. *Climate Change 2013: The Physical Science Basis. Contribution of Working Group I to the Fifth Assessment Report of the Intergovernmental Panel on Climate Change*; Cambridge University Press: Cambridge, United Kingdom and New York, NY, USA, 2013, p 1535.

(8) Marina-Montes, C.; Pérez-Arribas, L. V.; Escudero, M.; Anzano, J.; Cáceres, J. O. *Science of The Total Environment* **2020**, *721*, 137702.
(9) Hallquist, M.; Wenger, J. C.; Baltensperger, U.; Rudich, Y.; Simpson, D.; Claeys, M.; Dommen, J.; Donahue, N. M.; George, C.; Goldstein, A. H.; Hamilton, J. F.; Herrmann, H.; Hoffmann, T.; Iinuma, Y.; Jang, M.; Jenkin, M. E.; Jimenez, J. L.; Kiendler-Scharr, A.; Maenhaut, W.; McFiggans, G., et al. *Atmos. Chem. Phys.* **2009**, *9*, 5155-5236.
(10) Cajiao, D.; Albertos, B.; Tejedo, P.; Muñoz-Puelles, L.; Garilleti, R.; Lara, F.; Sancho, L. G.; Tirira, D. G.; Simón-Baile, D.; Reck, G. K.; Olave, C.; Benayas, J. *Journal of Environmental Management* **2020**, *266*, 110593.
(11) IAATO. 2017.
(12) Osipov, E. Y.; Osipova, O. P.; Khodzher, T. V. *Geochemistry* **2019**, 125554.
(13) Legrand, M.; Preunkert, S.; Weller, R.; Zipf, L.; Elsässer, C.; Merchel, S.; Rugel, G.; Wagenbach, D. *Atmos. Chem. Phys.* **2017**, *17*, 14055-14073.
(14) Xu, G.; Chen, L.; Zhang, M.; Zhang, Y.; Wang, J.; Lin, Q. *Air Quality, Atmosphere & Health* **2019**, *12*, 271-288.
(15) Decesari, S.; Paglione, M.; Rinaldi, M.; Dall'Osto, M.; Simó, R.; Zanca, N.; Volpi, F.; Facchini, M. C.; Hoffmann, T.; Götz, S.; Kampf, C. J.; O'Dowd, C.; Ceburnis, D.; Ovadnevaite, J.; Tagliavini, E. *Atmos. Chem. Phys.* **2020**, *20*, 4193-4207.
(16) Cáceres, J. O.; Sanz-Mangas, D.; Manzoor, S.; Pérez-Arribas, L. V.; Anzano, J. *Science of The Total Environment* **2019**, *665*, 125-132.
(17) Marina-Montes, C.; Pérez-Arribas, L. V.; Anzano, J.; Cáceres, J. O. *Atmosphere* **2020**, *11*.
(18) Sobanska, S.; Falgayrac, G.; Rimetz-Planchon, J.; Perdrix, E.; Brémard, C.; Barbillat, J. *Microchemical Journal* **2014**, *114*, 89-98.
(19) Zhang, Q.; Jimenez, J. L.; Canagaratna, M. R.; Ulbrich, I. M.; Ng, N. L.; Worsnop, D. R.; Sun, Y. *Anal Bioanal Chem* **2011**, *401*, 3045-3067.
(20) Cheng, H.; Dong, X.; Yang, Y.; Feng, Y.; Wang, T.; Tahir, M. A.; Zhang, L.; Fu, H. *Journal of Environmental Sciences* **2021**, *100*, 11-17.
(21) Craig, R. L.; Nandy, L.; Axson, J. L.; Dutcher, C. S.; Ault, A. P. *J. Phys. Chem. A* **2017**, *121*, 5690-5699.
(22) Eom, H. J.; Gupta, D.; Cho, H. R.; Hwang, H. J.; Hur, S. D.; Gim, Y.; Ro, C. U. *Atmos. Chem. Phys.* **2016**, *16*, 13823-13836.
(23) Gupta, D.; Eom, H. J.; Cho, H. R.; Ro, C. U. *Atmos. Chem. Phys.* **2015**, *15*, 11273-11290.
(24) Sze, S. K.; Siddique, N.; Sloan, J. J.; Escribano, R. *Atmospheric Environment* **2001**, *35*, 561-568.
(25) Feng, Y.; Liu, L.; Yang, Y.; Deng, Y.; Li, K.; Cheng, H.; Dong, X.; Li, W.; Zhang, L. *Science of The Total Environment* **2019**, *685*, 189-196.
(26) Goldstein, J. I.; Newbury, D. E.; Echlin, P.; Joy, D. C.; Lyman, C. E.; Lifshin, E.; Michael, J. R., Newbury, D. E., Echlin, P., Joy, D. C., Lyman, C. E., Lifshin, E., … Michael, J. R., Ed.; Springer US, 2003.
(27) Toporski, J.; Dieing, T.; Hollricher, O.; Springer International Publishing, 2018.
(28) Cardell, C.; Guerra, I. *TrAC Trends in Analytical Chemistry* **2016**, *77*, 156-166.
(29) DIN-EN-12341. In:Standard, E. (Ed.), DIN EN 12341, 2014, p 57.
(30) Castro, K.; Pérez-Alonso, M.; Rodríguez-Laso, M. D.; Fernández, L. A.; Madariaga, J. M. *Anal Bioanal Chem* **2005**, *382*, 248-258.
(31) Lafuente, B.; Downs, R. T.; Yang, H.; Stone, N. In *Highlights in Mineralogical Crystallography*, 2016, pp 1-29.
(32) Bokobza, L.; Bruneel, J.-L.; Couzi, M. *C* **2015**, *1*.
(33) Soewono, A.; Rogak, S. *Aerosol Science and Technology* **2011**, *45*, 1206-1216.
(34) Ferrugiari, A.; Tommasini, M.; Zerbi, G. *Journal of Raman Spectroscopy* **2015**, *46*, 1215-1224.
(35) García-Florentino, C.; Gomez-Nubla, L.; Huidobro, J.; Torre-Fdez, I.; Ruíz-Galende, P.; Aramendia, J.; Hausrath, E. M.; Castro, K.; Arana, G.; Madariaga, J. M. *Astrobiology* **2021**.

(36) Prieto-Taboada, N.; Gómez-Laserna, O.; Martínez-Arkarazo, I.; Olazabal, M. Á.; Madariaga, J. M. *Anal. Chem.* **2014**, *86*, 10131-10137.
(37) Prieto-Taboada, N.; Fdez-Ortiz de Vallejuelo, S.; Veneranda, M.; Marcaida, I.; Morillas, H.; Maguregui, M.; Castro, K.; De Carolis, E.; Osanna, M.; Madariaga, J. M. *Scientific Reports* **2018**, *8*, 1613.
(38) Wollmann, G.; Freyer, D.; Voigt, W. *Monatshefte für Chemie - Chemical Monthly* **2008**, *139*, 739-745.
(39) Frost, R. L. *Journal of Raman Spectroscopy* **2011**, *42*, 1130-1134.
(40) Parker, S. F.; Zhong, L. *Royal Society Open Science* **2018**, *5*, 171574.
(41) Zapata, F.; Ortega-Ojeda, F.; García-Ruiz, C.; González-Herráez, M. *Sensors* **2018**, *18*, 2196.
(42) Eichler, J.; Weikusat, C.; Wegner, A.; Twarloh, B.; Behrens, M.; Fischer, H.; Hörhold, M.; Jansen, D.; Kipfstuhl, S.; Ruth, U.; Wilhelms, F.; Weikusat, I. *Frontiers in Earth Science* **2019**, *7*.
(43) Zhang, M.; Chen, L.; Xu, G.; Lin, Q.; Liang, M. *Journal of the Atmospheric Sciences* **2015**, *72*, 4629-4642.
(44) Bao, H.; Campbell, D. A.; Bockheim, J. G.; Thiemens, M. H. *Nature* **2000**, *407*, 499-502.
(45) Kumar, S.; Gopinathan, R.; Chandra, G. K.; Umapathy, S.; Saini, D. K. *Anal Bioanal Chem* **2020**, *412*, 2505-2516.

Supplementary Materials

Characterization of atmospheric aerosols in the Antarctic region using Raman Spectroscopy and Scanning Electron Microscopy

César Marina-Montes[a], Luis V. Pérez-Arribas[b], Jesús Anzano[a], Silvia Fdez-Ortiz de Vallejuelo[c], Julene Aramendia[c], Leticia Gómez-Nubla[c], Alberto de Diego[c], Juan Manuel Madariaga[c], Jorge O. Cáceres[*b]

[a] Laser Lab, Chemistry & Environment Group, Department of Analytical Chemistry, Faculty of Sciences, University of Zaragoza. Pedro Cerbuna 12, 50009 Zaragoza, Spain

[b] Laser Chemistry Research Group, Department of Analytical Chemistry, Faculty of Chemistry, Complutense University of Madrid. Plaza de Ciencias 1, 28040 Madrid, Spain

[c] Department of Analytical Chemistry, Faculty of Science and Technology, University of the Basque Country UPV/EHU. Leioa, Spain

*Corresponding author. Jorge O. Cáceres. E-mail: jcaceres@ucm.es (J.O. Cáceres).

Figure S1

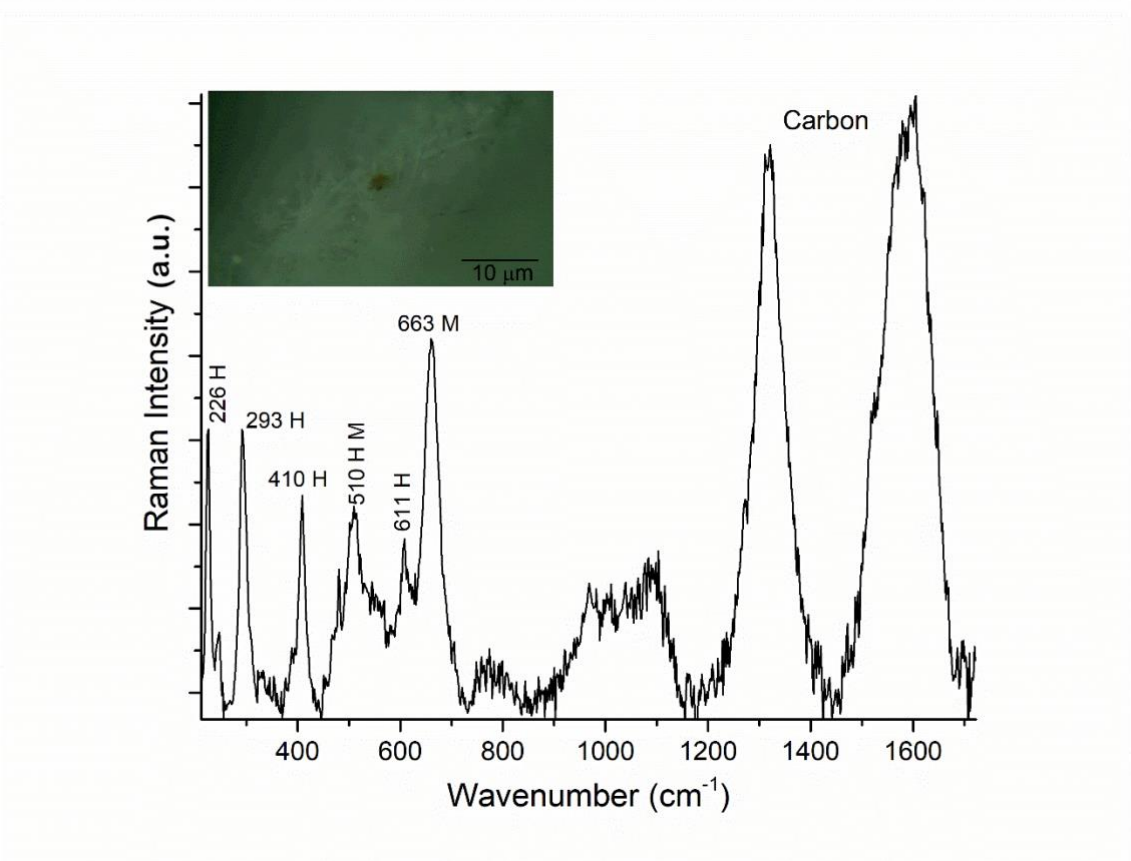

Figure S1. Raman spectrum where three minerals, hematite (Fe2O3) (H), magnetite (Fe3O4) (M), and carbon, are simultaneously present in a particle of a diameter greater than 30 microns that inhibits the appearance of the Raman background of the filter materials from an Antarctic aerosol sample.

Figure S2

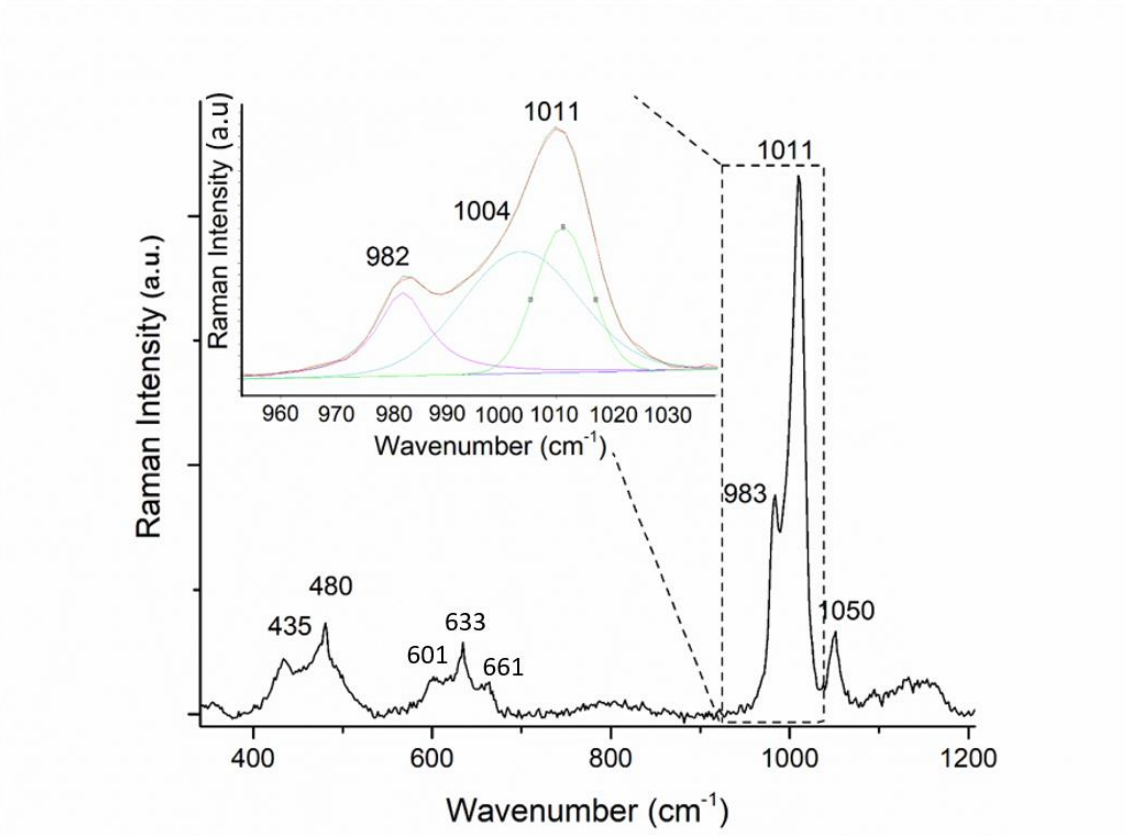

Figure S2. Raman spectrum of a clustered Antarctic particle with syngenite, gypsum+basanite and nitrocalcite**.** the main signals around 1000 cm^{-1} were decomposed in individual bands. This mathematical treatment lead to the conclusion that syngenite ($K_2Ca(SO_4)_2 \cdot H_2O$, Raman bands at 601, 633, 661, 982 and 1004cm^{-1}) was present [1], together with gypsum ($CaSO_4 \cdot 2H_2O$, main Raman band at 1008 cm^{-1}) probably mixed with basanite ($CaSO_4 \cdot ½H_2O$, main Raman band at 1017 cm^{-1}) [2]. Moreover, the band at 1050 cm^{-1} shows a FWHM=25 cm^{-1}, that belongs to nitrocalcite ($Ca(NO_3)_2 \cdot 4H_2O$) [3]

Figure S3

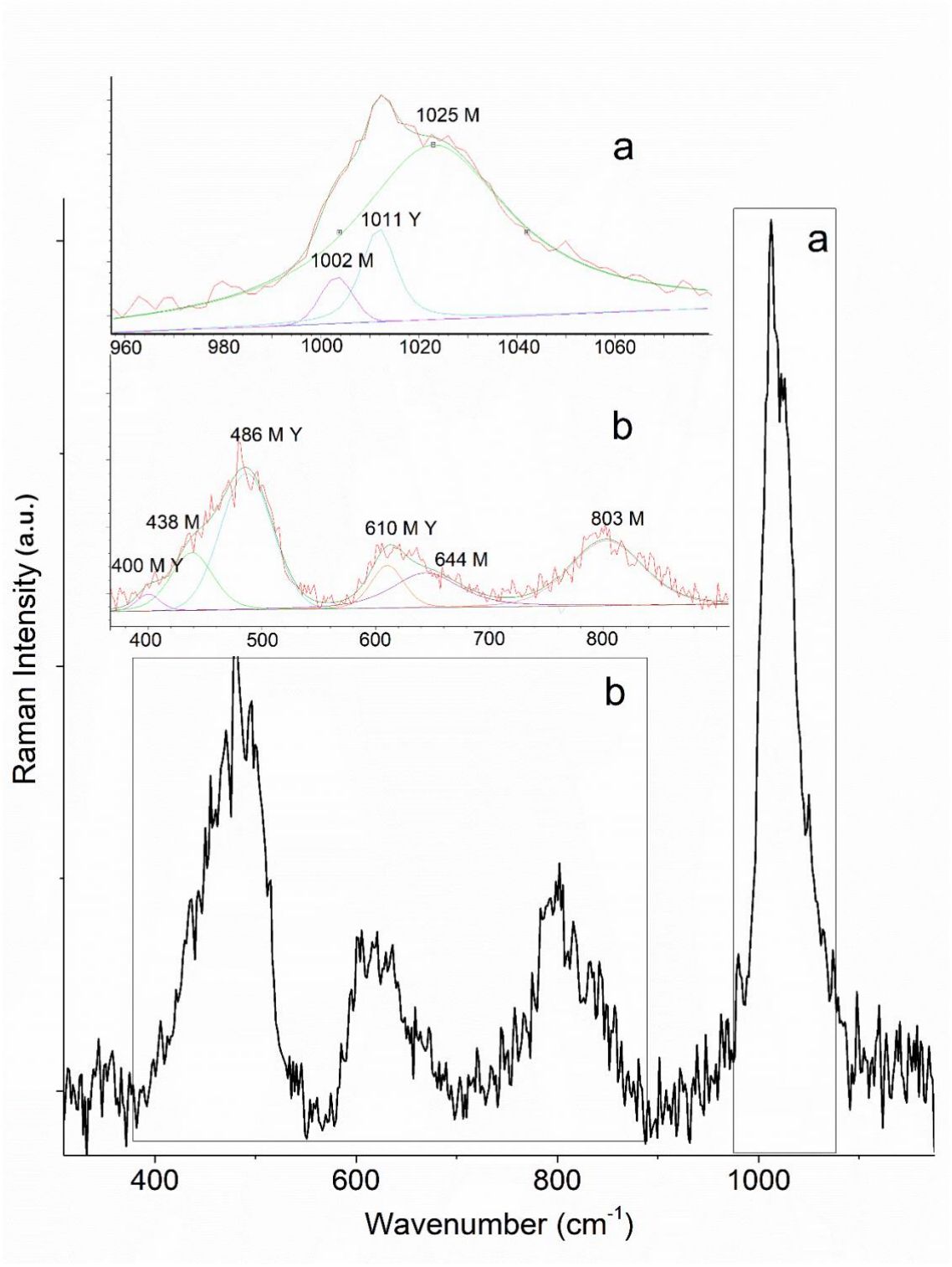

Figure S3. Raman spectrum of a white particle containing magnesio-copiapite (M), (MgFe3+4(SO4)6(OH)2.20H2O main Raman bands at 1002 and 1025 cm-1), and gypsum and basanite (Y) due to the signal at 1011 cm-1. The main (b) and the secondary broad bands were decomposed in individual bands to help in the identification of the minerals simultaneously present in the complex particle.

Table S1.

Spectrum	C	O	Na	Mg	Si	Cl	Cu	Al	Ca	Ti	Fe
B (BC)	38 ±1	37 ± 1	2.55 ± 0.05	0.41 ± 0.08	17.46 ± 0.06	2.8 3± 0.02	0.81 ± 0.01	<LQ	<LQ	<LQ	<LQ
C (NaCl)	<LQ	36 ± 1	30.24 ± 0.05	<LQ	6.61 ± 0.06	26.44 ± 0.02	<LQ	<LQ	<LQ	<LQ	<LQ
D (SiO_2)	<LQ	62 ± 2	8.81 ± 0.05	<LQ	22.11 ± 0.06	6.73 ± 0.02	<LQ	<LQ	<LQ	<LQ	<LQ
E (Fe Oxide)	8.7 ± 0.2	53 ± 1	2.43 ± 0.05	2.55± 0.08	17.82 ± 0.06	0.66 ± 0.02	0.73 ± 0.01	5.58 ± 0.01	3.08 ± 0.01	0.88 ± 0.08	4.51 ± 0.01

Table S1. Element weight (%) obtained by Energy – Dispersive Spectrum K_α analysis of Antarctic PM samples. Filter samples were coated with Au film.

Figure S4

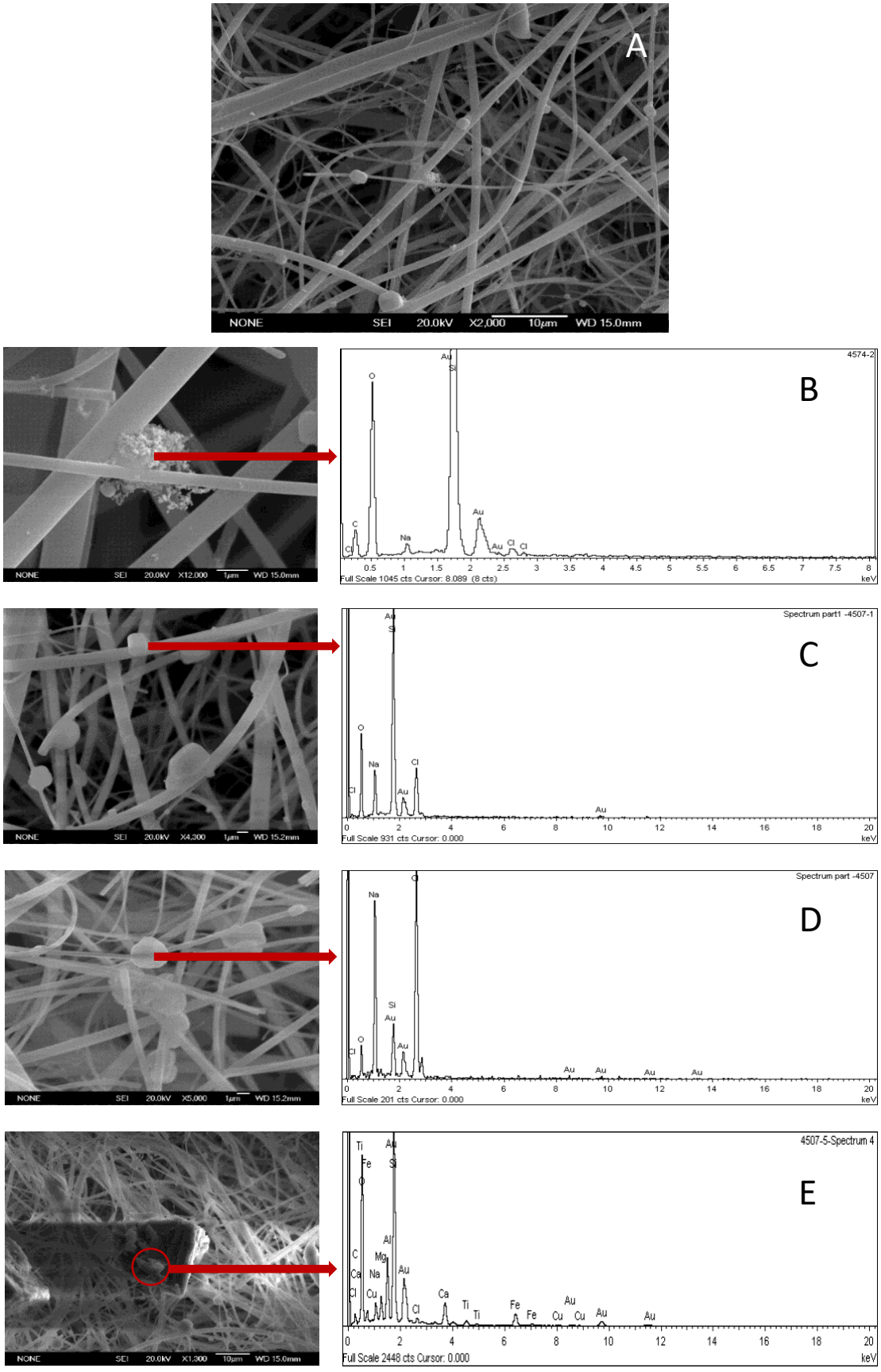
A
NONE SEI 20.0kV X2,000 10µm WD 15.0mm
B
4574-2
Au
Si
O
C
Cl
Na
Au
Au
Cl
Cl
0.5 1 1.5 2 2.5 3 3.5 4 4.5 5 5.5 6 6.5 7 7.5 8
Full Scale 1045 cts Cursor: 8.089 (8 cts)
keV
NONE SEI 20.0kV X12,000 1µm WD 15.0mm
C
Spectrum part1 -4507-1
Au
Si
O
Na
Cl
Cl
Au
Au
0 2 4 6 8 10 12 14 16 18 20
Full Scale 931 cts Cursor: 0.000
keV
NONE SEI 20.0kV X4,300 1µm WD 15.2mm
D
Spectrum part -4507
Na
Cl
Si
Au
O
Cl
Au
Au
Au
Au
Au
0 2 4 6 8 10 12 14 16 18 20
Full Scale 201 cts Cursor: 0.000
keV
NONE SEI 20.0kV X5,000 1µm WD 15.2mm
E
4507-5-Spectrum 4
Ti
Au
Fe
Si
O
C
Al
Mg
Ca
Na
Au
Cl
Cu
Ca
Ti
Ti
Fe
Fe
Au
Cu
Cu
Au
Au
0 2 4 6 8 10 12 14 16 18 20
Full Scale 2448 cts Cursor: 0.000
keV
NONE SEI 20.0kV X1,300 10µm WD 15.0mm

Figure S4. SEM-EDS spectra: (A) General morphological overview of PM particles in the quartz fiber filter; (B) Black Carbon particle and amorphous shape; (C) Sodium Chloride particle and tablet-like shape; (D) Quartz particle; (E) Iron oxide particle with traces of elements such as C, Na, Mg, Si, Cl, Cu, Al, Ca and Ti.

References

[1] C. García-Florentino, L. Gomez-Nubla, J. Huidobro, I. Torre-Fdez, P. Ruíz-Galende, J. Aramendia, E.M. Hausrath, K. Castro, G. Arana, J.M. Madariaga, Interrelationships in the Gypsum–Syngenite–Görgeyite System and Their Possible Formation on Mars, Astrobiology, (2021).
[2] N. Prieto-Taboada, O. Gómez-Laserna, I. Martínez-Arkarazo, M.Á. Olazabal, J.M. Madariaga, Raman Spectra of the Different Phases in the CaSO4–H2O System, Anal. Chem., 86 (2014) 10131-10137.
[3] N. Prieto-Taboada, S. Fdez-Ortiz de Vallejuelo, M. Veneranda, I. Marcaida, H. Morillas, M. Maguregui, K. Castro, E. De Carolis, M. Osanna, J.M. Madariaga, Study of the soluble salts formation in a recently restored house of Pompeii by in-situ Raman spectroscopy, Scientific Reports, 8 (2018) 1613.